



CHORUS

This is the accepted manuscript made available via CHORUS. The article has been published as:

Topological superconducting phase in the vicinity of ferromagnetic phases

Yuan-Yuan Xiang, Wan-Sheng Wang, Qiang-Hua Wang, and Dung-Hai Lee

Phys. Rev. B **86**, 024523 — Published 26 July 2012

DOI: [10.1103/PhysRevB.86.024523](https://doi.org/10.1103/PhysRevB.86.024523)

Topological superconductivity in the vicinity of ferromagnetic phases

Yuan-Yuan Xiang,¹ Wan-Sheng Wang,¹ Qiang-Hua Wang,¹ and Dung-Hai Lee^{2,3}

¹*National Lab of Solid State Microstructures, Nanjing University, Nanjing, 210093, China*

²*Department of Physics, University of California at Berkeley, Berkeley, CA 94720, USA*

³*Materials Sciences Division, Lawrence Berkeley National Laboratory, Berkeley, CA 94720, USA*

Through the study of concrete models we establish a strong tie between topological superconductivity and ferromagnetic spin correlations. Our result can be used as a guideline for the search of topological superconductors whose pairing symmetry is invariant under time reversal. The results are obtained by the functional renormalization group method.

PACS numbers: 74.20.-z, 74.20.Rp, 71.27.+a

I. INTRODUCTION

Topological insulators and superconductors have become a focus of interest in condensed matter physics.^{1,2} These states are characterized by symmetry protected gapless boundary excitations. The existence of these excitations reflects the fact that it is impossible to smoothly connect a topological insulator/superconductor with its non-topological counterpart without crossing a quantum phase transition. Under the assumption of no electron-electron interaction, topological superconductors and insulators have been classified into ten symmetry classes^{3,4}. In each spatial dimension precisely five of these classes have topological representatives. Examples of topological insulators include the time reversal symmetry breaking (T-breaking) integer quantum Hall insulator⁵, and the time reversal invariant (T-invariant) topological insulators in two⁶ and three⁷ dimensions. Examples of topological superfluid/superconductor include the T-breaking ³He-A⁸ and Sr₂RuO₄⁹, and the T-invariant ³He-B⁸.

In this fast growing field discovering new topological materials is clearly very important. While many topological insulators have been predicted and experimentally confirmed^{1,2,7}, there is no conclusive evidence that topological superconductivity with time reversal invariant pairing symmetry is realized in any material. The recently discovered Cu_xBi₂Se₃¹⁰⁻¹² is an intriguing but not yet confirmed candidate. This makes the theoretical study of physical conditions that favor T-invariant topological superconductivity a pressing task.

Predicting topological superconductors is much harder than predicting topological insulators. This is because knowing the desired Bogoliubov de Gennes (BdG) band structure¹³ only meets half of the challenge. The other half requires the knowledge the microscopic interactions which favor the desired BdG band structure as the mean-field theory. Leaving topology aside, it is hard enough to predict superconductivity itself. This is because the energy scale involved in Cooper pairing is usually much smaller than the characteristic energies (e.g., the bandwidth) of the normal state. However in the last five years various types of renormalization group methods have been used to compute the *effective interaction* responsible for the Cooper pairing in iron-based

superconductors.^{14,15} In this paper we apply a similar method to study topological superconductivity.

In the literature there are many interesting proposals for inducing topological superconductivity via the proximity effect.¹⁶⁻¹⁹ (A notable exception is the intriguing proposal of Ref.¹².) In these proposals, pairing is artificially induced by a (non-topological) superconductor. The reason the induced superconducting state is topological is due to the novel spin-orbit coupled electron wavefunctions in the normal state. The focus of this paper is on materials which will be a topological superconductor by itself.

There are two classes (DIII and CI according to Ref.⁴) of T-invariant topological superconductor in three dimensions.^{3,4} They are differentiated by the transformation properties with respect to time reversal and particle-hole conjugation. In this paper we will focus on class DIII, for it has realization in space dimension $d = 1, 2$ and 3 . We ask “*under what condition is T-invariant topological superconductivity favored?*” We shall argue that it is when the ferromagnetic (to be precise small wavevector magnetic) fluctuations are strong.

Due to practical limitations (on computation) we shall limit ourselves to two dimensional, i.e., thin film topological superconductors. Such systems inevitably break the spatial inversion symmetry because of the presence of the Rashba spin-orbit coupling term near the surface. As a result the superconductors under consideration are *non-centrosymmetric*. For this type of superconductors parity even and parity odd pairing symmetries can mix. Many real superconducting materials are non-centrosymmetric. Examples include CePt₃Si²⁰, CeRhSi₃²¹, CeIrSi₃²², and the superconductivity found at the interface of LaAlO₃ and SrTiO₃²³. For discussions of topological pairing in centrosymmetric systems see, e.g., Ref.²⁴, and for non-centrosymmetric systems see, e.g., Ref.²⁵

Using functional renormalization group method, we establish a tie between topological superconductivity and ferromagnetic fluctuations. We provide different mechanisms that lead to strong ferromagnetic fluctuations and thence triplet pairing. Under such a condition, we show that a small Rashba coupling can induce T-invariant topological superconductivity. Our result implies that such a topological pairing is unlikely in superconducting

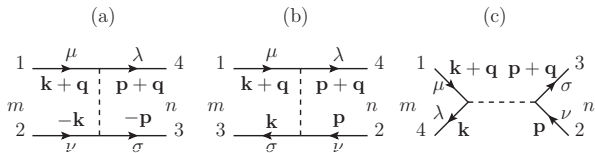


FIG. 1: A generic 4-point vertex Γ_{1234} is rearranged into P -, C -, and D -channels in (a)-(c), respectively. Here $\mathbf{k}, \mathbf{q}, \mathbf{p}$ are momenta, $\mu, \nu, \sigma, \lambda$ are spin indices, and m, n denote the form factors. On each side of the diagrams, the spin (and sublattice) labels are absorbed into the form factor labels wherever applicable (see the main text).

materials where singlet pairing dominates. The paper concludes with a guideline and few suggestions for systems that might realize T-invariant topological superconductivity.

The rest of this paper is structured as follows. In Sec.II we describe briefly the functional renormalization group method for our purpose, leaving the more technical details in the Appendix. In Sec.III and IV we provide two concrete models that lead to T-invariant topological superconductivity. In Sec.V we discuss the results and the relevance to experiments.

II. METHOD

Technically this work requires us to generalize the functional renormalization group (FRG) approach^{14,15,26,27} to Hamiltonians without spin rotation symmetry. In addition, because the necessity to study small momentum transfer particle-hole scatterings we use a Matsubara frequency rather than momentum cutoff. All calculations are carried out using the singular-mode functional renormalization group (SM-FRG) method.^{27,28} More details on this method can be found in the Appendix.

Consider a generic fully-antisymmetrized irreducible 4-point vertex function Γ_{1234} in $\Psi_1^\dagger \Psi_2^\dagger (-\Gamma_{1234}) \Psi_3 \Psi_4$. Here 1, 2, 3, 4 represent momentum and spin (and sublattice) indices. Figs.1(a)-(c) are rearrangements of Γ_{1234} into the pairing (P), crossing (C) and direct (D) channels each characterized by a collective momentum \mathbf{q} . In each channel the vertex function is decomposed as Eq. (A1) in the Appendix. There $\{f_m\}$ is a set of orthonormal lattice form factors.²⁹ The spin (and sublattice) indices are contained in the label of the form factors as shown in Figs.1(a)-(c). The decomposition in Eq. (A1) is exact if the form factors are complete, but a few of them are often enough to capture the leading instabilities.^{27,28} The FRG flow equations for P, C and D as a function of the cutoff scale Λ are given by Eqs. (A3), (A4) and (A5) in the Appendix. The effective interaction in the particle-particle (pp) and particle-hole (ph) channels are given, respectively, by $V_{pp} = -P/2$ and $V_{ph} = C$. [Because of antisymmetry $D (= -C)$ does not yield any new information.] During the FRG flow we monitor

the singular values of the matrix functions $V_{pp/ph}(\mathbf{q})$. The most negative singular values, $S_{pp/ph}$, occur at special momenta $\mathbf{q}_{pp/ph}$. While \mathbf{q}_{pp} is usually zero, \mathbf{q}_{ph} can evolve under RG before settling down to fixed values. The eigen function associated with S_{pp} is used to construct the gap function. Further details can be found in the Appendix.

III. TOPOLOGICAL PAIRING IN THE VICINITY OF VAN HOVE SINGULARITY

We consider spin-1/2 fermions hopping on a square lattice. The Hamiltonian is given by

$$H = \sum_{\mathbf{k}} \Psi_{\mathbf{k}}^\dagger [\epsilon(\mathbf{k})\sigma_0 + \lambda\vec{\gamma}(\mathbf{k}) \cdot \vec{\sigma}] \Psi_{\mathbf{k}} + U \sum_i n_{i\uparrow} n_{i\downarrow}. \quad (1)$$

Here $\Psi^\dagger = (\psi_\uparrow^\dagger, \psi_\downarrow^\dagger)$, $\epsilon(\mathbf{k}) = -2t(\cos k_x + \cos k_y) - 4t' \cos k_x \cos k_y - \mu$ is the normal state dispersion (t and t' are hopping amplitudes and μ is the chemical potential), i labels the lattice sites, and $n_{i\sigma} = \psi_{i\sigma}^\dagger \psi_{i\sigma}$. In addition, σ_0 is the 2×2 identity matrix and $\vec{\sigma}$ denotes the three Pauli matrices. In the Rashba spin-orbit coupling we consider $\vec{\gamma}(\mathbf{k}) = (-\sin k_y, \sin k_x, 0)$.

Combining the time-reversal and point group (C_{4v} in the present case) symmetries, it can be shown that the Cooper pair operator $B^\dagger = \sum_{\mathbf{k}} \Psi_{\mathbf{k}}^\dagger \Delta_{\mathbf{k}} \Psi_{-\mathbf{k}}^{\dagger T}$ takes the form,³⁰ $\Delta(\mathbf{k}) = [\phi(\mathbf{k})\sigma_0 + \vec{d}(\mathbf{k}) \cdot \vec{\sigma}]i\sigma_2$, where $\vec{d}(\mathbf{k})$ transforms, under the point group, like the product of $\phi(\mathbf{k})$ and $\vec{\gamma}(\mathbf{k})$. In the cases we have studied, to a good approximation, we can write

$$\Delta(\mathbf{k}) = [\phi(\mathbf{k})\sigma_0 + \chi(\mathbf{k})\hat{\gamma}(\mathbf{k}) \cdot \vec{\sigma}]i\sigma_2, \quad (2)$$

where $\hat{\gamma}(\mathbf{k}) = \vec{\gamma}(\mathbf{k})/|\vec{\gamma}(\mathbf{k})|$, $\phi(\mathbf{k})$ and $\chi(\mathbf{k})$ are even functions of \mathbf{k} and are real up to a global phase. They transform according to the same irreducible representation of the point group (for multi-dimensional representations there are several ϕ and χ 's). In Landau theory, ϕ and χ act as order parameters, and can induce each other in the presence of the Rashba coupling ($\lambda \neq 0$).

It is important to note that the Rashba term splits each of the otherwise spin-degenerate Fermi surface into two. The spin split Fermi surfaces are characterized by eigen values ± 1 of $\hat{\gamma}(\mathbf{k}) \cdot \vec{\sigma}$. In the case where $\phi(\mathbf{k})$ and $\chi(\mathbf{k})$ are nodeless, the gap function on the two split Fermi surfaces will have opposite sign if the magnitudes of $\chi(\mathbf{k})$ dominates over $\phi(\mathbf{k})$. It turns out that for *each pair* of Fermi pockets surrounding a T-invariant \mathbf{k} point the above sign reversal leads to two counter-propagating Majorana edge modes. *Thus topological pairing requires the triplet χ -component to be dominant.* Moreover sign reversal (in the gap function) on an odd/even pairs of the spin-split Fermi surfaces (satisfying the condition specified above) will lead to strong/weak topological superconductivity.

For $t' = -0.475t$, $\mu = -2t$ and $\lambda = 0.01t$, the spin-split Fermi surfaces are shown in Fig.2(a). They are pointy

along \hat{x} and \hat{y} , reflecting the existence of saddle points (van Hove singularities) on the Brillouin zone boundary. These features lead to enhanced ferromagnetic correlations via the Stoner mechanism. However, this mechanism over-estimates the spin fluctuations by ignoring the overlaps to the other channels. The FRG method we apply here treats all channels on equal footing, and provides a mechanism of triplet pairing due to enhanced ferromagnetic fluctuations. The form factors used in our SM-FRG extend up to second neighbors in real space.²⁹ The RG flow of $S_{pp/ph}$ is shown in Fig.2(b) for $U = 2.5t$. The arrows associated with the S_{ph} flow record the \mathbf{q}_{ph} evolution from $\mathbf{q}_1 = (\pi, \pi)$ to $\mathbf{q}_2 = 0$. By inspecting the spin structure of the \mathbf{q}_2 -singular mode we find it corresponds to ferromagnetic fluctuation. The increased ferromagnetic fluctuation around \mathbf{q}_2 enhances pairing in the triplet channel via their mutual overlaps (see Appendix). The gap function is determined by the singular mode associated with S_{pp} at the diverging cutoff scale. The result is a dominant χ -component together with a much smaller ϕ -component. The corresponding gap function on the two Fermi surfaces is shown in Fig.2(a) (gray scale). A sign change is clearly visible. According to the established criterion,² this pairing state is topological. To verify this, we calculate the BdG energy spectrum using the obtained pairing form factor in a strip geometry (open-boundary along \hat{x}). The resulting eigen energies as a function of $q = k_y$ is shown in Fig.2(c). There are two in-gap counter propagating Majorana edge modes associated with each edge.

Had we turned off the Rashba coupling, the leading pairing channel (p -wave) would be two-fold degenerate (with dominant amplitudes on 1st neighbor bonds). Under this condition even an infinitesimal Rashba coupling breaks the degeneracy by linearly recombining the p -waves into $\Delta(\mathbf{k}) = i \sin k_x \sigma_0 + \sin k_y \sigma_3$, or $\chi(\mathbf{k}) = |\vec{\gamma}(\mathbf{k})|$ in Eq. (2), leading to a gap function $\pm\chi(\mathbf{k})$ on the infinitesimally split Fermi surfaces. Interestingly this gap function has the same symmetry as the two dimensional version of the ^3He B phase. In addition, the Rashba coupling plays a similar role as the parity -invariant spin-orbit interaction in ^3He : they both lift the degeneracy in the pairing channel.

Fig.2(d) is a phase diagram of the present model, defined by the upper critical scale in the pp- and ph-channels. With t' and μ fixed, we find that for $U < 2.77t$ the system is in the topological triplet superconducting state, while the ferromagnetic spin-density-wave (SDW) state is realized for $U > 2.77t$.

IV. TOPOLOGICAL PAIRING ENHANCED BY INTER-POCKET SCATTERING

In this section we show another route to topological pairing. In this case pairing is triggered by inter-Fermi surface scattering in a way similar to the pairing in the

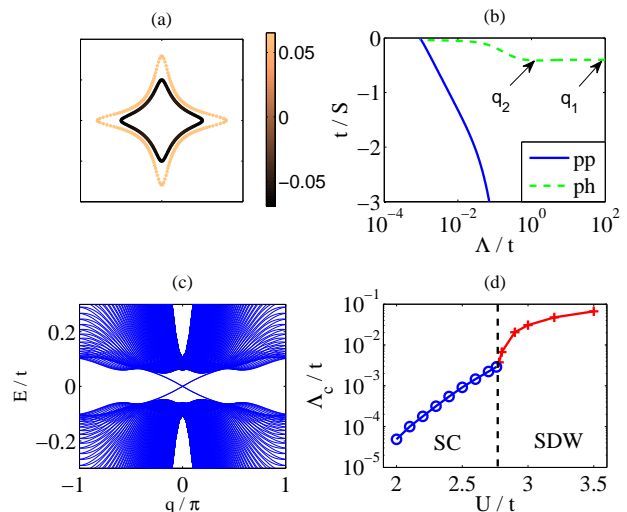


FIG. 2: (Color online) (a) The spin-split Fermi surfaces. The color scale shows the values of the gap functions. The spin-splitting is intentionally enlarged for a better view. (b) The SM-FRG flow of $S_{pp/ph}$ versus cutoff scale Λ . Arrows mark the evolution of the wave vector in the ph-channel during the RG flow. (c) The low energy BdG eigen spectrum in a strip (open along \hat{x}) as a function of the momentum $q\hat{y}$. (d) The phase diagram defined by the upper critical scale in the pp- and ph-channels as a function of U . The vertical dashed line marks the phase boundary.

pnictides.^{14,15}

Consider a honeycomb lattice. The single particle Hamiltonian is given by

$$H_0 = - \sum_{i\delta} \Psi_i^\dagger t_\delta \Psi_{i+\delta} - i\lambda \sum_{i\delta_{nn}} \Psi_i^\dagger (\hat{z} \times \vec{\delta}_{nn} \cdot \vec{\sigma}) \Psi_{i+\delta_{nn}} - \mu \sum_i \Psi_i^\dagger \Psi_i. \quad (3)$$

Here i labels lattice sites, δ runs over the 1st and 2nd neighbor bonds, with $t_\delta = t, t'$. The spin-dependent hopping, the Rashba term, is limited to the nearest neighbor bonds δ_{nn} . Choosing a lattice site as the origin, the point group is C_{3v} . For the SM-FRG calculation, we choose the form factors up to the 2nd neighbors.²⁹ (Since the honeycomb lattice has two sites per unit cell the labels of the form factors in Fig.1 include the sublattice indices.²⁷) The Fermi surfaces for $t' = 0.357t$, $\lambda = 0.02t$ and $\mu = 1.664t$ are shown in Fig.3(a). There are a few interesting features of the band structure that are worth noting (1) The Fermi surfaces encircle either the zone center (Γ) or the zone corners (K and K'). However only Γ is T-invariant, hence according to Ref.² only the Γ -Fermi surfaces are topologically relevant. (2) The Γ and K -pockets have close by segments, hence allow small momentum transfer particle-hole scattering. If such scattering is magnetic, it corresponds to nearly ferromag-

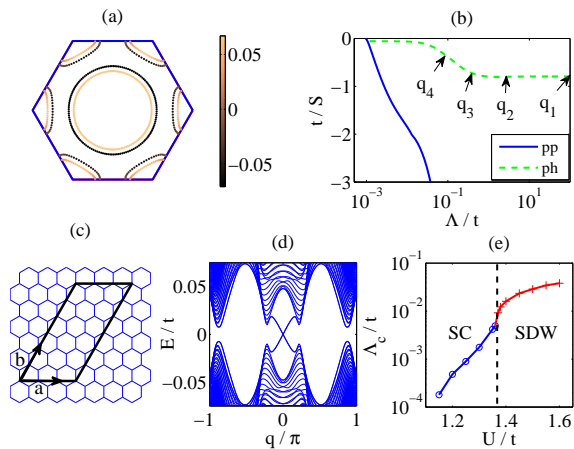


FIG. 3: (Color online) (a) The Fermi pockets and the associated gap functions (gray scale, in units of t). The spin-splitting between each pair of Fermi pockets is enlarged for clarity. The hexagon is the zone boundary. (b) The SM-FRG flow of $S_{pp/ph}$ versus the cutoff scale Λ . Arrows mark sharp changes of \mathbf{q}_{ph} during the RG flow. (c) A strip (marked by the thick lines) open along \mathbf{a} and periodic along \mathbf{b} directions (\mathbf{a} and \mathbf{b} are parallel to the primitive lattice vectors). (d) The low energy BdG eigen spectrum for (c) as a function of the conserved momentum q along \mathbf{b} . (e) The phase diagram defined by the upper critical scale in the pp- and ph-channels as a function of U . The vertical dashed line marks the phase boundary.

netic fluctuations, hence can induce triplet and topological pairing.

In the following we show for $U = 1.26t$ this is exactly what happens. During the RG flow shown in Fig.3(b), the strength of S_{ph} increases and \mathbf{q}_{ph} evolves from $\mathbf{q}_1 = (0.667, 1.152)\pi$ to $\mathbf{q}_2 = 0$, $\mathbf{q}_3 = (0.250, 0.048)\pi$ and finally settles down at $\mathbf{q}_4 = (0.333, 0.192)\pi$. We have checked that \mathbf{q}_4 corresponds to the scattering between near by parallel segments between the Γ and K pockets. Inspection of the spin structure of the singular mode associated with $\mathbf{q}_{2,3,4}$ reveals that they corresponds to spin fluctuations. As such fluctuations are enhanced, they causes S_{pp} to grow in magnitude and eventually diverge at a relatively high critical scale. The resulting gap function is shown in Fig.3(a) in gray scale. It is *fully gapped on all Fermi surfaces*, and have opposite sign on each pair of spin-split pockets. Since the K-pockets are topologically irrelevant, the sign change between the Γ Fermi surfaces implies the pairing is strong-topological. To verify this we consider a strip schematically shown in Fig.3(c). It is open along \mathbf{a} and periodic along \mathbf{b} directions. The BdG energy spectrum as a function of the momentum $q = \mathbf{k} \cdot \hat{\mathbf{b}}$ is shown in Fig.3(d). There are two branches of Majorana modes at each edge. Fig.3(e) is a phase diagram for the present model with fixed μ . The topological superconducting phase is realized for $U < 1.365t$, while ferromagnetic-like SDW instability is realized for

$U > 1.365t$.

V. DISCUSSION

Thus in both of the above examples we have seen

- small momentum magnetic fluctuations
- \Rightarrow degenerate triplet pairing, and
- degenerate triplet pairing + Rashba coupling
- \Rightarrow topological pairing.

We notice that in each case there is a finite range in the parameter space where topological pairing is realized. The fact that ferromagnetic fluctuations enhance triplet pairing has a long history. These include the works on the pairing of ^3He ,^{8,31,32} and the extension of the Kohn-Luttinger theorem to p -wave pairing for 2D and 3D electron gas in the dilute limit.^{33,34} Examples of works on lattice systems include³⁵⁻³⁷

It is important to emphasize that if pairing is predominantly singlet a weak Rashba coupling can only induce a small triplet component, hence is insufficient to induce the desired sign change in the gap function. Of course this does not rule out the possibility of topological pairing in the presence of strong spin-orbit interaction.

Many non-centrosymmetric superconductors appear near antiferromagnetic rather than the ferromagnetic phase. These include CePt_3Si , CeRhSi_3 , CeIrSi_3 and CeCoGe_3 . For these materials topological superconductivity is unlikely. There are also many materials where superconductivity appears near ferromagnetism. Examples include $\text{Li}_2\text{Pd}_3\text{B}$, $\text{Li}_2\text{Pt}_3\text{B}$, URhGe , HoMo_6Se_8 , ErRh_4B_4 ,³⁸ iron under pressure,³⁹ and the interface superconductivity of $\text{LaAlO}_3/\text{SrTiO}_3$.²³ In these systems it should be more likely to find topological pairing.

In conclusion, our functional renormalization group investigations indicates that T-invariant topological superconductivity in symmetry class DIII should occur in systems close to the ferromagnetic (or small wavevector magnetic) instability. Bandstructure wise, in the absence of Rashba coupling, these systems should have an odd number of spin-degenerate Fermi pockets (each enclosing a T-invariant momentum) in order for strong topological pairing to occur.

Acknowledgments

QHW acknowledges the support by NSFC (under grant No.10974086, No.10734120 and No.11023002) and the Ministry of Science and Technology of China (under grant No.2011CBA00108 and 2011CB922101). DHL acknowledges the support by the DOE grant number DE-AC02-05CH11231.

VI. APPENDIX

Here we provide the technical details of the SM-FRG method.^{27,28} We begin by reviewing the definition of the vertex functions used in the main text. Consider a generic fully-antisymmetrized irreducible 4-point vertex function Γ_{1234} in $\Psi_1^\dagger \Psi_2^\dagger (-\Gamma_{1234}) \Psi_3 \Psi_4$. Here 1, 2, 3, 4 represent momentum and spin (and sublattice) indices. Figs.4(a)-(c) are rearrangements of Γ_{1234} into the pairing (P), crossing (C) and direct (D) channels each characterized by a collective momentum \mathbf{q} . The rest momentum dependence of the vertex function can be decomposed as,

$$\begin{aligned} \Gamma_{\mathbf{k}+\mathbf{q}, -\mathbf{k}, -\mathbf{p}, \mathbf{p}+\mathbf{q}}^{\mu\nu\sigma\lambda} &\rightarrow \sum_{mn} f_m^*(\mathbf{k}) P_{mn}(\mathbf{q}) f_n(\mathbf{p}), \\ \Gamma_{\mathbf{k}+\mathbf{q}, \mathbf{p}, \mathbf{k}, \mathbf{p}+\mathbf{q}}^{\mu\nu\sigma\lambda} &\rightarrow \sum_{mn} f_m^*(\mathbf{k}) C_{mn}(\mathbf{q}) f_n(\mathbf{p}), \\ \Gamma_{\mathbf{k}+\mathbf{q}, \mathbf{p}, \mathbf{p}+\mathbf{q}, \mathbf{k}}^{\mu\nu\sigma\lambda} &\rightarrow \sum_{mn} f_m^*(\mathbf{k}) D_{mn}(\mathbf{q}) f_n(\mathbf{p}). \end{aligned} \quad (\text{A1})$$

Here $\{f_m\}$ is a set of orthonormal lattice form factors. The spin (and sublattice) indices are contained in the label of the form factors as shown in Figs.4(a)-(c). The decomposition in Eq. (A1) is exact if the form factors are complete, but in practice a few of them are often enough to capture the leading instabilities.^{27,28} Because of full antisymmetry, the matrices C and D satisfy $D = -C$, and are therefore not independent. In the following D is used for bookkeeping purpose.

Ignoring the spin and sublattice labels for the moment, the form factors are given by

$$f_m(\mathbf{k}) = \sum_{\mathbf{r}} f_m(\mathbf{r}) \exp(-i\mathbf{k} \cdot \mathbf{r}), \quad (\text{A2})$$

where $f_m(\mathbf{r})$ transforms according to an irreducible representation of the point group, and \mathbf{r} is the bond vectors connecting the two Ψ 's (or two Ψ^\dagger 's) in Fig.4(a) and one Ψ and one Ψ^\dagger in Fig.4(b) and (c). In our calculation we choose form factors up to the 2nd neighbor bonds. We have checked that longer range form factors does not change the results qualitatively. To be specific, for square lattice, the real-space form factors we used are 1) $f_1 = 1$ for on-site; 2) $f_2 = 1/2$, $f_3 = (1/2) \cos 2\theta_{\mathbf{r}}$, $f_4 = \sqrt{1/2} \cos \theta_{\mathbf{r}}$, and $f_5 = \sqrt{1/2} \sin \theta_{\mathbf{r}}$ for 1st neighbors, where $\theta_{\mathbf{r}}$ is the azimuthal angle of \mathbf{r} ; 3) $f_6 = 1/2$, $f_7 = (1/2) \sin 2\theta_{\mathbf{r}}$, $f_8 = \sqrt{1/2} \cos(\theta_{\mathbf{r}} - \pi/4)$ and $f_9 = \sqrt{1/2} \sin(\theta_{\mathbf{r}} - \pi/4)$ for 2nd neighbors. For hexagonal lattices, the form factors we used are 1) $f_1 = 1$ for on-site; 2) $f_2 = \sqrt{1/3}$, $f_3 = \sqrt{2/3} \cos \theta_{\mathbf{r}}$ and $f_4 = \sqrt{2/3} \sin \theta_{\mathbf{r}}$ for 1st neighbors; 3) $f_5 = \sqrt{1/6}$, $f_6 = \sqrt{1/3} \cos \theta_{\mathbf{r}}$, $f_7 = \sqrt{1/3} \sin \theta_{\mathbf{r}}$, $f_8 = \sqrt{1/3} \cos 2\theta_{\mathbf{r}}$, $f_9 = \sqrt{1/3} \sin 2\theta_{\mathbf{r}}$, $f_{10} = \sqrt{1/6} \cos 3\theta_{\mathbf{r}}$ for 2nd neighbors. Notice that the

1st neighbor bonds stem from different sublattices are negative to each other.

In the case where sublattices are involved, the form factor label m also includes the sublattice indices associated

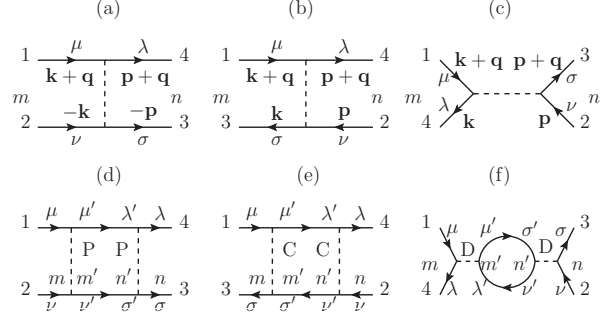


FIG. 4: A generic 4-point vertex Γ_{1234} is rearranged into P -, C -, and D -channels in (a)-(c), respectively. Here $\mathbf{k}, \mathbf{q}, \mathbf{p}$ are momenta, $\mu, \nu, \sigma, \lambda$ denote spins, and m, n denote the form factors. On each side of the diagrams, the spin (and sublattice) labels are absorbed into the form factor labels wherever applicable. The one-loop diagrams that contribute to ∂P , ∂C and ∂D are shown in (d)-(f), respectively.

with the two Ψ 's (or Ψ^\dagger 's), or the Ψ and Ψ^\dagger . However, once \mathbf{r} is fixed only one of these sublattice indices is independent. We include the independent sublattice index in the form factor label, $(m, a) \rightarrow m$. Here a labels, e.g., the fermion field 1 or 4 in Fig.4(a), 1 or 4 in (b), and 1 or 3 in (c). The sublattice index is an independent label because point group operations do not mix sublattices when the origin is chosen to be a lattice site.

The total number of form factors N in a calculation is determined by the number of real space neighbors, the number of sublattices and the four spin combinations $(\mu, \nu) = \uparrow\uparrow, \uparrow\downarrow, \downarrow\uparrow, \downarrow\downarrow$ associated with two Ψ (P channel) or the Ψ and Ψ^\dagger (C and D channels). Thus P , C and D are all $N \times N$ matrix functions of momentum \mathbf{q} .

The Feynman diagrams associated with one-loop contributions to the flow of the irreducible 4-point vertex function are given in Fig.4(d)-(f). They represent the partial changes ∂P , ∂C and ∂D , respectively. (Notice that the three diagrams in Fig.4(d)-(f) become the usual five diagrams in the spin-conserved case.) The internal Greens functions are convoluted with the form factors hence in matrix form,

$$\begin{aligned} \partial P / \partial \Lambda &= P \chi'_{pp} P / 2, \\ \partial C / \partial \Lambda &= C \chi'_{ph} C, \\ \partial D / \partial \Lambda &= -D \chi'_{ph} D \end{aligned} \quad (\text{A3})$$

where we have suppressed the dependence of the collective momentum \mathbf{q} , and

$$\begin{aligned}
(\chi'_{pp})_{mn} &= \frac{\partial}{\partial \Lambda} \int \frac{d\omega_n}{2\pi} \int \frac{d^2 \mathbf{p}}{S_{BZ}} f_m(\mathbf{p}) G(\mathbf{p} + \mathbf{q}, i\omega_n) G(-\mathbf{p}, -i\omega_n) f_n^*(\mathbf{p}) \theta(|\omega_n| - \Lambda) \\
&= -\frac{1}{2\pi} \int \frac{d^2 \mathbf{p}}{S_{BZ}} f_m(\mathbf{p}) G(\mathbf{p} + \mathbf{q}, i\Lambda) G(-\mathbf{p}, -i\Lambda) f_n^*(\mathbf{p}) + (\Lambda \rightarrow -\Lambda), \\
(\chi'_{ph})_{mn} &= \frac{\partial}{\partial \Lambda} \int \frac{d\omega_n}{2\pi} \int \frac{d^2 \mathbf{p}}{S_{BZ}} f_m(\mathbf{p}) G(\mathbf{p} + \mathbf{q}, i\omega_n) G(\mathbf{p}, i\omega_n) f_n^*(\mathbf{p}) \theta(|\omega_n| - \Lambda) \\
&= -\frac{1}{2\pi} \int \frac{d^2 \mathbf{p}}{S_{BZ}} f_m(\mathbf{p}) G(\mathbf{p} + \mathbf{q}, i\Lambda) G(\mathbf{p}, i\Lambda) f_n^*(\mathbf{p}) + (\Lambda \rightarrow -\Lambda), \tag{A4}
\end{aligned}$$

where G is the free fermion Greens function, S_{BZ} is the total area of the Brillouine zone. Here $\Lambda > 0$ is the infrared cutoff of the Matsubara frequency ω_n . As in usual FRG implementation, the self energy correction and frequency dependence of the vertex function are ignored.

Since ∂P , ∂C and ∂D come from independent one-loop diagrams, they contribute independently to the full $d\Gamma_{1234}$, which needs to be projected onto the three channels. Therefore the full flow equations are given by, formally,

$$\begin{aligned}
dP/d\Lambda &= \partial P/\partial \Lambda + \hat{P}(\partial C/\partial \Lambda + \partial D/\partial \Lambda), \\
dC/d\Lambda &= \partial C/\partial \Lambda + \hat{C}(\partial P/\partial \Lambda + \partial D/\partial \Lambda), \\
dD/d\Lambda &= \partial D/\partial \Lambda + \hat{D}(\partial P/\partial \Lambda + \partial C/\partial \Lambda), \tag{A5}
\end{aligned}$$

where \hat{P}, \hat{C} and \hat{D} are the projection operators in the sense of Eq. (A1). Here we have used the fact that $\hat{K}(\partial K) = \partial K$ for $K = P, C, D$. In Eq. (A5) the terms preceded by the projection operators represent the overlaps of different channels. For two channels to overlap, the spatial coordinates of all four fermion fields must lie within the range set of the form factors. In the actual calculation the projections in Eq.(A5) are preformed in real space.

The effective interaction in the particle-particle (pp) and particle-hole (ph) channels are given, respectively, by $V_{pp} = -P/2$ and $V_{ph} = C$. By singular value decomposition, we determine the leading instability in each channel,

$$V_X^{mn}(\mathbf{q}_X) = \sum_{\alpha} S_X^{\alpha} \phi_X^{\alpha}(m) \psi_X^{\alpha}(n), \tag{A6}$$

where $X = pp, ph$, S_X^{α} is the singular value of the α -th singular mode, ϕ_X^{α} and ψ_X^{α} are the right and left eigen vectors of V_X , respectively. We fix the phase of the eigen vectors by requiring $\text{Re}[\sum_m \phi_X^{\alpha}(m) \psi_X^{\alpha}(m)] > 0$ so that $S_X^{\alpha} < 0$ corresponds to an attractive mode in the X-channel.

In the pp-channel $\mathbf{q}_{pp} = 0$ corresponds to the zero center-of-mass momentum Cooper instability. The matrix gap function $\Delta_{\mathbf{k}}$ in the spin and sublattice basis is determined as follows. A singular mode ϕ_{pp}^{α} leads to a

pair operator (in the momentum space),

$$\Psi_{\mathbf{k}}^{\dagger} \Delta_{\mathbf{k}} \Psi_{-\mathbf{k}}^{\dagger T} = \sum_{m=(m,a,\mu,\nu)} \psi_{a\mu}^{\dagger}(\mathbf{k}) \phi_{pp}^{\alpha}(m) f_m(\mathbf{k})^* \psi_{a\nu}^{\dagger}(-\mathbf{k}). \tag{A7}$$

Here a is the independent sublattice index, and a_m is the second sublattice index determined by a and m as discussed earlier, and μ, ν are spin indices. The parity of $\Delta_{\mathbf{k}}$ under space inversion determines the singlet and triplet components. The gap function in the band eigen basis can be determined by the unitary transformation

$$\tilde{\Psi}_{\mathbf{k}}^{\dagger} = \Psi_{\mathbf{k}}^{\dagger} U_{\mathbf{k}}^{\dagger}, \tag{A8}$$

where the columns of $U_{\mathbf{k}}^{\dagger}$ are the Bloch states $\{|\mathbf{k}, n\rangle\}$ (n is the band index). Under Eq. (A8) the pairing matrix transforms into

$$\tilde{\Delta}_{\mathbf{k}} = U_{\mathbf{k}} \Delta_{\mathbf{k}} U_{-\mathbf{k}}^T. \tag{A9}$$

In the weak coupling case (i.e., when the magnitude of the superconducting gap is much smaller than the bandwidth), only the diagonal part of $\tilde{\Delta}$ (i.e., intra-Fermi surface pairing) is important. Since Eq. (A9) involves Bloch states at two different momenta, the phases of the associated Bloch states enters $\tilde{\Delta}$. Since there is time-reversal symmetry we fix the Bloch state phase at \mathbf{k} and $-\mathbf{k}$ by demanding $\hat{T}|\mathbf{k}, n\rangle = |-\mathbf{k}, n\rangle$ and $\hat{T}^2|\mathbf{k}, n\rangle = -|\mathbf{k}, n\rangle$, where $\hat{T} = i\sigma_2 K$ is the time-reversal operator.

In the particle-hole channel, we calculate the singular values associated with $V_{ph}(\mathbf{q})$ at all momenta \mathbf{q} . Unlike the Cooper channel, the most negative singular value can occur at non-zero momentum \mathbf{q}_{ph} . The associated particle-hole operator is given by

$$\Psi_{\mathbf{k}+\mathbf{q}}^{\dagger} \Pi_{\mathbf{k}} \Psi_{\mathbf{k}} = \sum_{m=(m,a,\mu,\nu)} \psi_{a\mu}^{\dagger}(\mathbf{k} + \mathbf{q}) \phi_{ph}^{\alpha}(m) f_m^*(\mathbf{k}) \psi_{a\nu}(\mathbf{k}). \tag{A10}$$

Usually the on-site form factor dominates in the particle-hole channel. By inspecting the spin structure of the on-site form factor one can easily determine whether the instability is charge or spin like.

- ¹ For a reviews see M. Z. Hasan and C. L. Kane, *Rev. Mod. Phys.* **82**, 3045 (2010).
- ² For a review see X.-L. Qi and S.-C. Zhang, *Rev. Mod. Phys.* **83**, 1057 (2011).
- ³ A. Y. Kitaev, *AIP Conf. Proc.* **1134**, 22 (2009).
- ⁴ A. P. Schnyder, S. Ryu, A. Furusaki, A. W. W. Ludwig, *Phys. Rev. B* **78**, 195125 (2008); *AIP Conf. Proc.* **1134**, 10 (2009); S. Ryu, A. P. Schnyder, A. Furusaki, A. W. W. Ludwig, *New Journal of Physics* **12**, 065010 (2010).
- ⁵ K. von Klitzing, G. Dorda, and M. Pepper, *Phys. Rev. Lett.* **45**, 494 (1980); D.J. Thouless, M. Kohmoto, M. P. Nightingale, and M. den Nijs, *Phys. Rev. Lett.* **49**, 405 (1982).
- ⁶ M. König, S. Wiedmann, C. Brüne, A. Roth, H. Buhmann, L. W. Molenkamp, X.-L. Qi, S.-C. Zhang, *Science* **318**, 766 (2007).
- ⁷ D. Hsieh, D. Qian, L. Wray, Y. Xia, Y. S. Hor, R. J. Cava, and M. Z. Hasan, *Nature* **452**, 970 (2008); D. Hsieh, Y. Xia, D. Qian, L. Wray, J. H. Dil, F. Meier, J. Osterwalder, L. Patthey, J. G. Checkelsky, N. P. Ong, A. V. Fedorov, H. Lin, A. Bansil, D. Grauer, Y. S. Hor, R. J. Cava, and M. Z. Hasan, *Nature*, **460**, 1101 (2009); D. Hsieh, Y. Xia, D. Qian, L. Wray, F. Meier, J. H. Dil, J. Osterwalder, L. Patthey, A. V. Fedorov, H. Lin, A. Bansil, D. Grauer, Y. S. Hor, R. J. Cava, and M. Z. Hasan, *Phys. Rev. Lett.* **103**, 146401 (2009); D. Hsieh, Y. Xia, L. Wray, D. Qian, A. Pal, J. H. Dil, J. Osterwalder, F. Meier, G. Bihlmayer, C. L. Kane, Y. S. Hor, R. J. Cava, and M. Z. Hasan, *Science* **323**, 919 (2009); Y. Xia, D. Qian, D. Hsieh, L. Wray, A. Pal, H. Lin, A. Bansil, D. Grauer, Y. S. Hor, R. J. Cava and M. Z. Hasan, *Nature Physics* **5**, 398 (2009); Y. L. Chen, J. G. Analytis, J.-H. Chu, Z. K. Liu, S.-K. Mo, X. L. Qi, H. J. Zhang, D. H. Lu, X. Dai, Z. Fang, S. C. Zhang, I. R. Fisher, Z. Hussain, Z.-X. Shen, *Science* **325**, 178 (2009).
- ⁸ For a review see D. Vollhardt, and P. Wölfle, *The Superfluid Phases of Helium* (Taylor and Francis, USA 1990).
- ⁹ For a review and references see A. P Mackenzie, and Y. Maeno, *Rev. Mod. Phys.* **75**, 657 (2003).
- ¹⁰ Y.S. Hor, A.J. Williams, J.G. Checkelsky *et al* *Phys. Rev. Lett.* **104**, 057001 (2010).
- ¹¹ S. Sasaki, M. Kriener, K. Segawa *et al*, *Phys. Rev. Lett.* **107**, 217001 (2011).
- ¹² Liang Fu and E. Berg, *Phys. Rev. Lett.* **105**, 097001 (2010).
- ¹³ A. P. Schnyder and S. Ryu, *Phys. Rev. B* **84**, 060504 (2011).
- ¹⁴ F. Wang, H. Zhai, Y. Ran, A. Vishwanath, D.-H. Lee, *Phys. Rev. Lett.* **102**, 047005 (2009); A. V. Chubukov, D. V. Efremov, I. Eremin, *Phys. Rev. B* **78**, 134512 (2008); R. Thomale, C. Platt, J. P. Hu, C. Honerkamp, B. A. Bernevig, *Phys. Rev. B* **80**, 180505 (2009); H. Zhai, F. Wang, and D.-H. Lee, *Phys. Rev. B* **80**, 064517 (2009).
- ¹⁵ For a review see Fa Wang and D.-H. Lee, *Science* **332**, 200 (2011).
- ¹⁶ Liang Fu, C. L. Kane, and E. J. Mele, *Phys. Rev. Lett.* **98**, 106803 (2007); Liang Fu and C. L. Kane, *ibid* **100**, 096407 (2008).
- ¹⁷ M.Sato, Y. Takahashi, and S. Fujimoto, *Phys. Rev. Lett.* **103**, 020401 (2009); J. D. Sau, R. M. Lutchyn, S. Tewari, and S. Das Sarma, *Phys. Rev. Lett.* **104**, 040502 (2010).
- ¹⁸ J. Alicea, *Phys. Rev. B* **81**, 125318 (2010).
- ¹⁹ J. Linder, Y. Tanaka, T. Yokoyama, A. Sudbø, and N. Nagaosa, *Phys. Rev. Lett.* **104**, 067001 (2010); J. Linder, Y. Tanaka, T. Yokoyama, A. Sudbø, and N. Nagaosa, *Phys. Rev. B* **81**, 184525 (2010).
- ²⁰ E. Bauer, G. Hilscher, H. Michor, Ch. Paul, E. W. Scheidt, A. Gribanov, Yu. Seropegin, H. Nöel, M. Sigrist, and P. Rogl, *Phys. Rev. Lett.* **92**, 027003 (2004).
- ²¹ N. Kimura, K. Ito, K. Saitoh, Y. Umeda, H. Aoki, and T. Terashima, *Phys. Rev. Lett.* **95**, 247004 (2005).
- ²² I. Sugitani, Y. Okuda, H. Shishido, T. Yamada, A. Thamizhavel, E. Yamamoto, T. D. Matsuda, Y. Haga, T. Takeuchi, R. Settai, and Y. ōnuki, *J. Phys. Soc. Jpn* **75**, 043703 (2006).
- ²³ N. Reyren, S. Thiel, A.D. Caviglia, L. F. Kourkoutis, G. Hammerl, C. Richter, C. W. Schneider, T. Kopp, A.-S. Rüetschi, D. Jaccard, M. Gabay, D. A. Muller, J.-M. Triscone, and J. Mannhart, *Science* **317**, 1196 (2007).
- ²⁴ G. E. Volovik and L. P. Gorkov, *Sov. Phys. JETP* **61**, 843 (1985).
- ²⁵ M. Sato, S. Fujimoto, *Phys. Rev. B* **79**, 094504 (2009); M. Sato, Y. Takahashi, and S. Fujimoto, *Phys. Rev. B* **82**, 134521 (2010); P. Ghosh, J. D. Sau, S. Tewari, and S. Das Sarma, *Phys. Rev. B* **82**, 184525 (2010); C. K. Lu and S. Yip, *Phys. Rev. B* **78**, 132502 (2008).
- ²⁶ C. Honerkamp, M. Salmhofer, N. Furukawa, and T. M. Rice, *Phys. Rev. B* **63**, 035109 (2001).
- ²⁷ Wan-Sheng Wang, Yuan-Yuan Xiang, Qiang-Hua Wang, Fa Wang, Fan Yang, and Dung-Hai Lee, *Phys. Rev. B* **85**, 035414 (2012).
- ²⁸ C. Husemann, and M. Salmhofer, *Phys. Rev. B* **79**, 195125 (2009).
- ²⁹ In real space (ignoring other labels), the form factors $\{f_m(\mathbf{r})\}$ are irreducible representations of the point group, where \mathbf{r} is the bond vector connecting lattice sites. Bond vectors connected by point group operations form a support for the form factor. For a given support, the number of independent form factors equals the number of independent bonds therein.
- ³⁰ For a review and references see M. Sigrist, *Lectures on the Physics of Strongly Correlated Systems XIII*, edited by A. Avella and F. Mancini, American Institute of Physics (2009).
- ³¹ A. Layzer and D. Fay, *Int. J. Magn.* **1**, 135 (1971)).
- ³² P. W. Anderson and W. F. Brinkman, *The Helium Liquids*, edited by J. G. M. Armitage and I. E. Farquhar (Academic, New York, 1975), pp. 315-416; P. W. Anderson *Phys. Rev. B* **30**, 1549 (1984).
- ³³ D. Fay and A. Layzer, *Phys. Rev. Lett.* **20**, 187 (1968).
- ³⁴ M. Yu. Kagan and A. V. Chubukov, *Pisma Zh. Eksp. Teor. Fiz.* **47**, 525 (1988); A. V. Chubukov, *Phys. Rev. B* **48**, 1097 (1993).
- ³⁵ A. V. Chubukov and J. P. Lu, *Phys. Rev. B* **46**, 11163 (1992).
- ³⁶ C. Honerkamp and M. Salmhofer, *Physica C* **408-410**, 302 (2004).
- ³⁷ Y. Hori and A. Goto, *Journal of Physics, Conference Series* **150**, 052072 (2009); S. Onari, R. Arita, K. Kuroki, and H. Aoki, *Phys. Rev. B* **70**, 094523 (2004); Z. Szabo and Z. Gulacsi, *Phil. Mag. Part B* **76:5**, 833 (1997).
- ³⁸ Dai Aoki and Jacques Flouquet, *J. Phys. Soc. Jpn.* **81**, 011003 (2012).

³⁹ Katsuya Shimizu, *et al*, NATURE **412**, 316 (2001).